LU TP 19-22
June 2019

EVENT GENERATORS AND LIGHT DARK MATTER

Michal Nowak

Department of Astronomy and Theoretical Physics, Lund University

Bachelor thesis supervised by Stefan Prestel
and co-supervised by Johannes Bellm

Abstract

Recently, a number of experiments have been proposed with the aim of finding light dark matter. In particular, the proposed LDMX experiment is meant to utilize electron scattering off metal nuclei to excite dark matter emissions. Motivated by this, we construct an event generator for electrons scattering off metal nuclei. The relevant kinematics are presented in detail. The matrix element for the t-channel single photon exchange is calculated from Feynman rules. To obtain cross-sections for the scatterings we employ Monte Carlo techniques, in particular importance sampling. We improve how realistic the events are by distributing the incoming momenta according to a Gaussian. The validity of the results is investigated by a number of tests. Finally, we present the results as a number of plots depicting relevant observable quantities such as differential cross-sections and scattering angles.

Populärvetenskapligt sammanfattning

Mörk materia upptäcktes redan på 1930-talet av astronomer via sin enorma gravitationella påverkan på galaxer. Trots detta, har alla försök att hitta dess beståndsdelar via experiment misslyckats. Ledande modeller för den mörka materians natur brukar beskriva den som uppbyggd av så kallade ”WIMP:s” (weakly interacting massive particles) som översätts till ungefär: ”svagt interagerande massiva partiklar”. I och med detta har nästan alla experiment letat efter just dessa, massiva, partiklar.

Nyligen har det föreslagits att andra slags experiment bör byggas, som letar efter mycket lättare mörk-materia partiklar. Det är dessa experiment och tillhörande modeller som är bakgrunden till detta projekt. Det gemensamma draget hos flera av dessa experiment är användandet av en elektronstråle som träffar ett metallblock för att excitera fram emissioner av mörk materia partiklar. Dessa kan då detekteras via antingen sönderfall till kända partiklar, eller via störningar i den förväntade distributionen av utgående elektroner.

I detta arbete skapar vi en så kallad ”event generator”, ett datorprogram som simulerar partikelkollisioner. Dess uppgift är att generera stora mängder simulerade elektron-atomkärnekollisioner och beräkna ett flertal tillhörande storheter. Detta för att skapa en modell för vad ett experiment kan se om det inte finns någon ”lätt” mörk materia, så att modellen kan jämföras med experimentell data. Nästa steg efter detta arbete skulle kunna vara en utbyggnad av programmet för att inkludera emissioner av just mörk materia.

Contents

1 Introduction

The motivation for this thesis is the conundrum of the nature of dark matter. Despite overwhelming astrophysical evidence, no conclusive observation of dark matter particles has ever been achieved. Most models of dark matter assume that it is composed of WIMPs, short for "weakly interacting massive particles" and thus most experiments have been looking for these type of particles.

Recently it has been proposed that it might be worthwhile to look for much lighter weakly interacting particles [1]. The authors of [1] argue that light dark matter (LDM) particles might be detectable by relatively simple detectors as they are thought to have a weak electromagnetic coupling. Furthermore, they claim that electrons excited by electromagnetic scatterings might radiate "dark photons" (A') that subsequently decay to e.g. electron-positron pairs. By observing distributions of scattered electrons behind beam dumps it is thought that these LDM particles might be detected.

The authors of [1] propose a number of experiments to investigate this. They all share a common characteristic: an electron beam is used to impact a tungsten target. The resulting scatterings might produce dark photons.

The simulation of such a process is the motivation of this thesis. This is done by construction of an event generator for t-channel electron - metal nucleus scatterings. The event generator can be found at [2] and can be used for reproducing the results presented in this thesis. We present in detail the underlying kinematics and calculate the relevant matrix element. We then describe the integrals that allow for calculation of observable quantities such as energy and cross-section. These integrals are computed numerically in the event-generator program [2], in anticipation of future improvements that might rule out analytical methods. We transform the integrals into forms suitable for Monte-Carlo integration.

In order to make the event generator more realistic, the focus of the project was shifted towards improving the electron-nucleus scattering simulation instead of modeling dark matter. In any real scenario, the particles in the target and in the beam have momenta that are distributed in a particular way due to e.g thermal and electromagnetic effects. To model this, the event generator distributes the incoming momenta according to a Gaussian, with the possibility of easily changing this to a different distribution.

The goal of this project is to create an event generator for electron-metal nucleus scattering. Furthermore, the idea is that it could be used as a framework by future students for generators that simulate LDM events.

2 Event Generator Theory

2.1 Brief Light Dark Matter Theory

The family of models of LDM considered by [1] and [3] describe the dark matter as being charged under a $U(1)$ field called "dark QED" [4] (denoted $U(1)_D$, the D stands for dark). The lagrangian of these dark matter models contains [4]:

$$\mathcal{L} \supset -\frac{1}{4}F^{'\mu\nu}F'_{\mu\nu} + \frac{1}{2}m^2_{A'}A^{'\mu}A'_{\mu} - A'_{\mu}\left(\epsilon e J^{\mu}_{\text{em}} + g_D J^{\mu}_D\right) \tag{2.1}$$

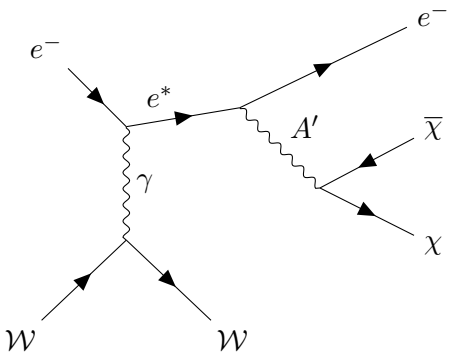

Figure 1: Feynman diagram depicting one of the processes that might enable dark matter detection. Time goes from left to right. The scattered electron (e^*) emits a dark photon which subsequently decays to an invisible particle - anti particle pair $\chi\overline{\chi}$. Diagram made using [5].

where $F'^{\mu\nu}$ is the field strength tensor of the new $U(1)_D$ force, A'^{μ} is the field of the new $U(1)_D$ gauge boson (the "dark photon"), $m_{A'}$ is the mass of the "dark" photon, J^{μ}_{em} is the regular electromagnetic current and J^{μ}_{D} is the new "dark" current. The scalar ϵ is the kinetic mixing parameter which determines the degree of the mixing between QED and dark QED. Finally, g_D is the $U(1)_D$ coupling constant.

From the second to last term we see that that the dark photon field A' couples to the electromagnetic current, albeit with a very small coupling controlled by ϵ. This means that e.g. an electron can radiate off an A' which gives a window into probing dark matter. One can look for such emissions by looking for missing momentum in a detector since the electron recoils as a result of the emission while the A' is invisible. The process is shown in fig. 1. It is also possible that the A' decays into light dark matter particles, denoted by χ (and its antiparticle $\overline{\chi}$ in some models). This can happen provided that $m_{A'} > 2m_{\chi}$. Since the χ remain invisible to the detector, we do not investigate this possibility further.

For experiments that attempt constraining such models by measuring the scattered electrons alone, it is crucial to accurately model all known, non-A' related, effects that affect the electron momentum. Only then can conclusive signal-versus-background statements be made.

2.2 Kinematics

In this chapter we develop the kinematics necessary for the processes that the event generator will simulate. The basic process modelled in the first part of the project is the electron-tungsten t-channel scattering, shown in fig. 2. Especially important are the four-momenta and their correspondence to incoming and outgoing particles.

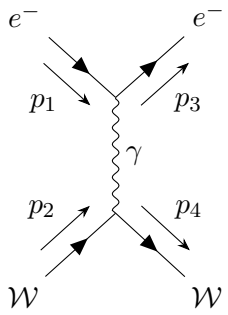

Figure 2: Diagram depicting the t-channel electron-tungsten scattering. Time goes from left to right. Free-standing arrows denote the four-momenta. Diagram made using [5].

The conditions at the experiment that we are modelling dictate what kinematic we will consider. Guided by [1], we consider $\mathcal{O}(10)$ GeV electron beam and tungsten atoms in the beam dump having only small thermal momenta. It is evident that the masses of the electrons can be neglected to good approximation. We have in the Lab-frame:

$$\begin{aligned} p_1 &= (\mathrm{p_e}, 0, 0, \mathrm{p_e}) \\ p_2 &= \left(\sqrt{\mathrm{p}_{\mathcal{W}}^2 + m_{\mathcal{W}}^2}, 0, 0, -\mathrm{p}_{\mathcal{W}}\right) \end{aligned} \tag{2.2}$$

where p_e is the absolute value of the incoming electron 3-momentum (taken for convenience to be initially along z-axis) and is $\mathrm{p}_{\mathcal{W}}$ is the same but for tungsten. To significantly simplify calculations we want to perform a Lorentz boost to the centre-of-momentum (CM) frame and thus obtain $p_1^* = (E_1, 0, 0, P^*)$ and $p_2^* = (E_2, 0, 0, -P^*)$ where the star superscript denotes a CM quantity. The required transformations are: $P^* = E_1 = \gamma\left(\mathrm{p}_e - v_{CM}\mathrm{p}_e\right)$, $E_2 = \gamma\left(\sqrt{\mathrm{p}_{\mathcal{W}}^2 + m_{\mathcal{W}}^2} - v_{CM}\mathrm{p}_{\mathcal{W}}\right)$ where the gamma factor and velocity of the CM in the lab frame are given by:

$$\begin{aligned} \gamma &= \frac{\sum E_{LAB}}{\sqrt{\left(\sum E_{LAB}\right)^2 - \left(\sum \mathbf{p}_{LAB}\right)^2}} = \frac{\mathrm{p}_e + \sqrt{\mathrm{p}_{\mathcal{W}}^2 + m_{\mathcal{W}}^2}}{\sqrt{\left(\mathrm{p}_e + \sqrt{\mathrm{p}_{\mathcal{W}}^2 + m_{\mathcal{W}}^2}\right)^2 - \left(\mathrm{p}_e + \mathrm{p}_{\mathcal{W}}\right)^2}} = \frac{\mathrm{p}_e + \sqrt{\mathrm{p}_{\mathcal{W}}^2 + m_{\mathcal{W}}^2}}{\sqrt{s}} \\ v_{CM} &= \frac{\left|\sum \mathbf{p}_{LAB}\right|}{\sum E_{LAB}} = \frac{\mathrm{p}_e + \mathrm{p}_{\mathcal{W}}}{\mathrm{p}_e + \sqrt{\mathrm{p}_{\mathcal{W}}^2 + m_{\mathcal{W}}^2}}. \end{aligned} \tag{2.3}$$

Here, the useful Mandelstam variable $s = (p_1 + p_2)^2$ was introduced. We can now write the incoming four-momenta in terms of Lorentz-invariant quantities:

$$\begin{aligned} P^* = E_1 &= \frac{1}{\sqrt{s}}\left(\mathrm{p}_e\sqrt{\mathrm{p}_{\mathcal{W}}^2 + m_{\mathcal{W}}^2} - \mathrm{p}_e\mathrm{p}_{\mathcal{W}}\right) = \frac{s - m_{\mathcal{W}}^2}{2\sqrt{s}} \\ E_2 &= \frac{1}{\sqrt{s}}\left(\mathrm{p}_e\sqrt{\mathrm{p}_{\mathcal{W}}^2 + m_{\mathcal{W}}^2} + m_{\mathcal{W}}^2 - \mathrm{p}_e\mathrm{p}_{\mathcal{W}}\right) = \frac{s + m_{\mathcal{W}}^2}{2\sqrt{s}}. \end{aligned} \tag{2.4}$$

Following the scattering, the outgoing momenta will in general not be along the z-axis. We choose to write the resulting four-vectors in terms of the angles ϕ (azimuthal angle) and θ

(transverse angle), defined as usual in spherical coordinates (see Figure 3). We also assume that the nucleus is not excited and thus has the same mass as before the scattering.

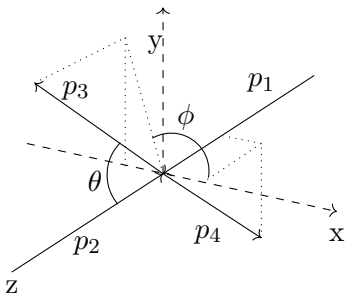

Figure 3: The set-up and coordinates of the collision in the CM frame.

Using standard parametrization from spherical to Cartesian coordinates, we get that the outgoing momenta are (in the CM frame):

$$\begin{aligned}\mathbf{p}_3 &= P^* \left(\sin\theta\cos\phi, \sin\theta\sin\phi, \cos\theta\right) \\ \mathbf{p}_4 &= P^* \left(\sin(\pi-\theta)\cos(\pi+\phi), \sin(\pi-\theta)\sin(\pi+\phi), \cos(\pi-\theta)\right)\end{aligned} \tag{2.5}$$

In order to arrive at measurable quantities, we want to boost back to the LAB frame when our calculations are done. This is done conveniently when the four-momenta are expressed in terms of invariant quantities. We already have the energy and momentum of the incoming particles written this way (c.f. eq. (2.4)). From eq. (2.5) we know that we can express the outgoing four-momenta in terms of ϕ (which is trivial), θ, E_2 and P^*. Hence we would like to write θ in terms of invariant quantities. From the definition of the Mandelstam variable t:

$$\begin{aligned}&t = (p_1 - p_3)^2 = m_1^2 + m_2^2 - 2p_1p_3 = -2(E_1 \cdot E_3 - \mathbf{p}_1\mathbf{p}_3) = \\ &= -2\left(E_1^2 - P^{2,*}\cos\theta\right) = \frac{\left(s - m_{\mathcal{W}}^2\right)^2}{2s}(\cos\theta - 1) \Leftrightarrow \\ &\theta = \arccos\left(\frac{2st}{\left(s - m_{\mathcal{W}}^2\right)^2} + 1\right)\end{aligned} \tag{2.6}$$

Evidently, t is a negative quantity. This is inconvenient for the event generator program considered later, so we will make use of the relation $-|t| = t$ in the generator. We also see that the minimum value of t is that of $t_{min} = -4E_1^2$ when $\theta = \pi$ (i.e. back scattering). Correspondingly, the maximum value of t is $t_{max} = 0$ when $\theta = 0$.

Finally, we can boost back to Lab frame. Using the inverse Lorentz transformations:

$$\begin{aligned}\mathrm{p}_{3,z} &= \gamma\left(\mathrm{p}_{3,z}^* + v_{CM}E_3^*\right) \\ \mathrm{p}_{4,z} &= \gamma\left(\mathrm{p}_{4,z}^* + v_{CM}E_4^*\right) \\ E_3 &= \gamma\left(E_3^* + v_{CM}\mathrm{p}_{3,z}^*\right) \\ E_4 &= \gamma\left(E_4^* + v_{CM}\mathrm{p}_{4,z}^*\right)\end{aligned} \tag{2.7}$$

making use of the the invariant quantities stated previously the first momentum becomes:

$$\mathrm{p}_{3,z} = \frac{\mathrm{p}_e + \sqrt{\mathrm{p}_{\mathcal{W}}^2 + m_{\mathcal{W}}^2}}{\sqrt{s}} \frac{\left(s - m_{\mathcal{W}}^2\right)}{2\sqrt{s}} \left(\left(1 + \frac{2st}{\left(s - m_{\mathcal{W}}^2\right)^2}\right) + \frac{\mathrm{p}_e + \mathrm{p}_{\mathcal{W}}}{\mathrm{p}_e + \sqrt{\mathrm{p}_{\mathcal{W}}^2 + m_{\mathcal{W}}^2}}\right) \tag{2.8}$$

where we used that $\mathrm{p}^*_{3,z} = E^*_3 \cos\theta$. The rest of eq. (2.7) can be rewritten similarly. With this, we have shown the full kinematics of the process.

2.3 Scattering & Matrix Element

As stated in the introduction, we want to model the underlying electron-tungsten scattering before the introduction of LDM emission can be made in future extensions of the code. This way we would see how such emission modifies the scattering. We thus want to calculate the matrix element associated with fig. 2 and use it to calculate cross-sections and outgoing momenta distributions. From fig. 2 we see and using the Feynman rules that the associated matrix element is:

$$\mathcal{M}_{1/2} = \frac{ie^2 Q}{t}\bar{u}(p_3)\gamma^\mu u(p_1)\bar{v}(p_4)\gamma_\mu v(p_2) \tag{2.9}$$

The subscript 1/2 emphasizes that the tungsten is treated as a spin 1/2 fermion, something that will be investigated later. We now follow the procedure for obtaining the squared matrix element as described in detail in [6]. Averaging and summing over spins and squaring it:

$$\left|\overline{\mathcal{M}_{1/2}}\right|^2 = \frac{1}{4}\sum_{spins}\left|\mathcal{M}_{1/2}\right|^2 = \frac{e^4Q^2}{4t^2}\,\mathrm{tr}\left[(\not{p}_3 + m_e)\gamma^\mu(\not{p}_1 + m_e)\gamma^\nu\right]\mathrm{tr}\left[(\not{p}_4 + m_{\mathcal{W}})\gamma_\mu(\not{p}_2 + m_{\mathcal{W}})\gamma_\nu\right] \tag{2.10}$$

Evaluating the first trace:

$$\begin{aligned}
&\mathrm{tr}\left[(\not{p}_3 + m_e)\gamma^\mu(\not{p}_1 + m_e)\gamma^\nu\right] = \mathrm{tr}\left[\not{p}_3\gamma^\mu\not{p}_1\gamma^\nu + \not{p}_3\gamma^\mu m_e\gamma^\nu + m_e\gamma^\mu\not{p}_1\gamma^\nu + m_e^2\gamma^\mu\gamma^\nu\right] = \\
&= 4m_e^2 g^{\mu\nu} + \mathrm{tr}\left[p_{3,\rho}p_{1,\sigma}\gamma^\rho\gamma^\mu\gamma^\sigma\gamma^\nu\right] = 4m_e^2 g^{\mu\nu} + 4p_{3,\rho}p_{1,\sigma}\left(g^{\rho\mu}g^{\sigma\nu} - g^{\rho\sigma}g^{\mu\nu} + g^{\rho\nu}g^{\mu\sigma}\right) = \\
&= 4\left(p_3^\mu p_1^\nu - p_3^\sigma p_{1,\sigma}g^{\mu\nu} + p_3^\nu p_1^\mu + m_e^2 g^{\mu\nu}\right)
\end{aligned} \tag{2.11}$$

and similarly for the other trace, $\mathrm{tr}\left[(\not{p}_4 + m_{\mathcal{W}})\gamma_\mu(\not{p}_2 + m_{\mathcal{W}})\gamma_\nu\right] = 4\left(p_{4,\mu}p_{2,\nu} + p_{4,\nu}p_{2,\mu} + \right.$ $\left. + g_{\mu\nu}\left(m_e^2 - p_4^\sigma p_{2,\sigma}\right)\right)$. Setting $m_e = 0$ and multiplying the traces together:

$$\begin{aligned}
&4\left(p_3^\mu p_1^\nu - p_3^\sigma p_{1,\sigma}g^{\mu\nu} + p_3^\nu p_1^\mu\right)\cdot 4\left(p_{4,\mu}p_{2,\nu} + p_{4,\nu}p_{2,\mu} + g^{\mu\nu}\left(m_{\mathcal{W}}^2 - p_4^\sigma p_{2,\sigma}\right)\right) = \\
&= 32\left((p_3\cdot p_4)(p_1\cdot p_2) + (p_1\cdot p_4)(p_3\cdot p_2) - m_{\mathcal{W}}^2(p_3\cdot p_1)\right)
\end{aligned} \tag{2.12}$$

which gives the following expression for the squared matrix element:

$$\left|\overline{\mathcal{M}_{1/2}}\right|^2 = \frac{8e^4Q^2}{t^2}\left((p_3\cdot p_4)(p_1\cdot p_2) + (p_1\cdot p_4)(p_3\cdot p_2) - m_{\mathcal{W}}^2(p_3\cdot p_1)\right). \tag{2.13}$$

It is convenient to introduce the Mandelstam variables to simplify subsequent computations. Using the results of the previous section and remembering that $p_1^2 = p_3^2 = 0$ since we have set $m_e = 0$:

$$\begin{aligned}
s &= (p_1 + p_2)^2 = 2p_1p_2 + p_2^2 \\
s &= (p_3 + p_4)^2 = 2p_3p_4 + p_4^2 \\
u &= (p_2 - p_3)^2 = p_2^2 - 2p_2p_3 \\
u &= (p_1 - p_4)^2 = p_4^2 - 2p_1p_4 \\
t &= (p_1 - p_3)^2 = -2p_1p_3 = -|t|
\end{aligned} \tag{2.14}$$

expanding eq. (2.13) and matching terms gives:

$$|\overline{\mathcal{M}_{1/2}}|^2 = \frac{8e^4Q^2}{t^2}\left(\left(\frac{s}{2}\right)^2 + \left(\frac{u}{2}\right)^2 + \frac{1}{2}m_{\mathcal{W}}^2\left(m_{\mathcal{W}}^2 - s - u + t\right)\right). \tag{2.15}$$

From the form of eq. (2.15) we see that it diverges as $t \to 0$. This is to be expected from quantum field theory as it corresponds to the emission of soft photons almost co-linearly with the (lightly) scattered electron. Experimentally this corresponds to the electrons that have undergone little to no scattering and emerge from the collision nearly parallel to the z-axis in Figure 3. Hence they are in general not measured by experiments anyway. We want to avoid producing events with a t too close to 0. To do so we include a "cut" on the variable t i.e. we set a highest allowed value for it, t_{max} (t_{min} is determined by s and corresponds to back-scattering). However, t is a rather abstract quantity and it would be nice to have a more tangible way of determining what the cut actually does and which value of t_{max} to choose given experimental conditions. We do this in Appendix A by translating a cut on the scattering angle θ in the Lab frame to a cut on t_{max}.

So far, we have treated the tungsten as a fundamental spin 1/2 particle. Upon looking up the isotopes of tungsten present in nature we see that the majority of tungsten is actually of integer spin. The low energy limit is the same for integer and spin 1/2 particles, but we are considering high energy transfers in e.g. back-scattering. The matrix elements for spin 0 and 1 particles were calculated by J. Bellm using [7], [8] and we compare them for both low mass (1 GeV) and tungsten mass (180 GeV) scenarios. Spin 0:

$$|\overline{\mathcal{M}_0}|^2 = \frac{e^4Q^2}{t^2}\left(s^2 + u^2 - t^2 - 2su + 4tm_{\mathcal{W}}^2\right) \tag{2.16}$$

Spin 1:

$$\begin{aligned}|\overline{\mathcal{M}_1}|^2 = \frac{e^4Q^2}{3t^2m_{\mathcal{W}}^4}\,(\; & m_{\mathcal{W}}^4(12s^2 + 20st + 17t^2) - 2tm_{\mathcal{W}}^2(2s^2 + 3st + 2t^2) \\ & -4m_{\mathcal{W}}^6(6s + t) + 12m_{\mathcal{W}}^8 + st^2(s + t)\big)\end{aligned} \tag{2.17}$$

In fig. 4 we see the histogram of the quantity $t^2\frac{\mathrm{d}\sigma}{\mathrm{d}|t|}$ for the three spin cases, with low mass (1 GeV). The reason for multiplying by t^2 is to avoid the $1/t^2$ divergence and see the behavior of the matrix elements clearly. We see how the differential cross-sections behave very differently. However, as we increase the mass to the target mass of tungsten in fig. 5 we see that the three spin cases almost completely coincide. Therefore, the approximation we use where the tungsten is treated as a 1/2 fermion is valid. We will thus drop the subscript 1/2 from now on.

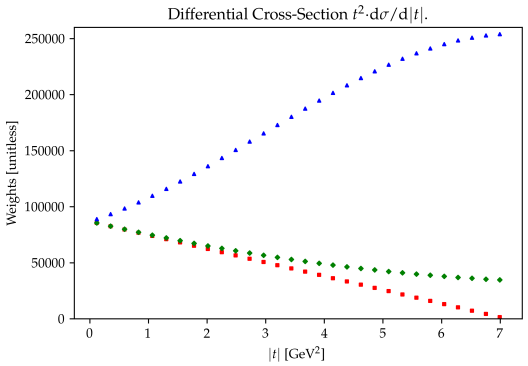

Figure 4: $t^2 \frac{d\sigma}{d|t|}$ for spin 0 (red squares), spin 1/2 (green diamonds) and spin 1 (blue triangles). The mass is low (1 GeV).

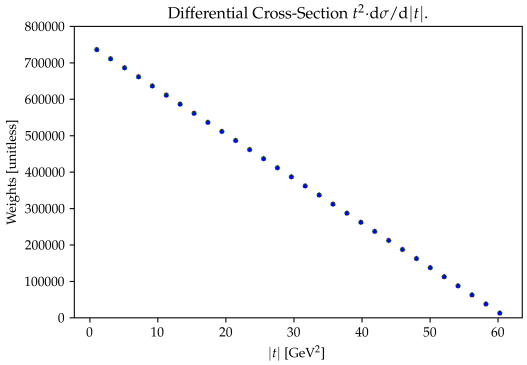

Figure 5: $t^2 \frac{d\sigma}{d|t|}$ for spin 0 (red squares), spin 1/2 (green diamonds) and spin 1 (blue triangles). The mass is the tungsten mass (180 GeV).

An additional issue the the treatment of the tungsten nucleus as a point charge. This is obviously not the case, the nucleus is an extended object which can in addition break up upon receiving a sufficiently energetic photon. Although no form factor is considered in this project, it can easily be added to the code of the event generator.

The nucleus is subject to different effects as the energy of the exchanged photon varies. The binding energy of a nucleus is $\mathcal{O}(10)$ MeV. For lower energies than that the nucleus can get excited if the exchanged photon has an energy corresponding to an excited state of the nucleus. The nucleon that has been excited to a higher orbital then promptly de-excites by emitting a γ. At energies above the binding energy one or more nucleons get kicked out. At even higher energies the exchanged γ starts to resolve the constituent quarks and we get deep inelastic scattering which breaks up the nucleus.

These effects can be approximately modeled by form factors. However, as the energies vary over large intervals it might be necessary to consider several different form factors (a form factor modelling an energy scale where the photon resolves the overall structure of the nucleus will be inadequate for energy scales where the quarks are resolved). A form factor that is commonly used in dark matter searches with tungsten target or detector material is the Helm form factor [9], [10] (see [11] for a typical example).

Does a form factor apply in our case? Based on the discussion above, we can be sure that it does if the energy of the photon is $\mathcal{O}(10)$ MeV or higher (since the photon starts to resolve the overall structure of the nucleus at lower energies, the form factor damping will actually begin at even lower energies). We can make an order of magnitude estimate by looking at how much energy the tungsten nucleus receives during the collision. The lowest energy case will of course be when $t = t_{max}$. Using the result of appendix A, we can calculate t_{max} with a 20°cut and a beam energy similar to that of LDMX, say 4 GeV [3]. This gives $t_{max} \approx 2$ GeV^2. Using the kinematics presented in the previous section we can calculate the total energy of the nucleus: $E_{\mathcal{W}} \approx 180.005$ GeV. Since this is an excess of the order of 10 MeV a form factor would be necessary for precise calculations. We do not include it, but leave a place for an arbitrary form factor in the code.

2.4 Monte Carlo Integrals

The basis for testing theory against experiment are experimentally measurable quantities such as cross section, outgoing transverse momentum distributions and energies. In order to test the LDM model, we would like to come up with predictions with how LDM emissions might affect measurable quantities in electron-metal scatterings. To do this, we need to first develop methods of obtaining the "nominal" cross-sections and other quantities. Once this is done, we can add dark matter to the process and see how the results change.

The fundamental quantity we are interested in is the cross-section, σ (subject to a cut on the scattering angle c.f. section 2.3), and the differential cross-section $\frac{\mathrm{d}\sigma}{\mathrm{d}t}$ where t is the usual Mandelstam invariant. The general formula for scattering of $2 \to n$ particles is [12]:

$$\sigma = \frac{I_n}{F_n} \tag{2.18}$$

where the velocity-dependent flux factor F can be rewritten in terms of invariants [12]:

$$F_n = 2\left(s - m_{\mathcal{W}}^2\right) \tag{2.19}$$

and the integral I_n is [12]:

$$I_n = \frac{1}{(2\pi)^{3n-4}} \int \prod_{i=1}^{n} \frac{\mathrm{d}^3 p_i}{2E_i} \delta^4 \left(p_a + p_b - \sum_i p_i\right) \left|\overline{\mathcal{M}}\right|^2 \tag{2.20}$$

In our case there are two outgoing particles, so $n = 2$ in all above equations. Simplifying, performing the ϕ integral and rewriting the above equations in terms of invariants [12] gives:

$$\begin{aligned} \frac{\mathrm{d}\sigma}{\mathrm{d}t} &= \frac{1}{16\pi\left(s - m_{\mathcal{W}}^2\right)^2} \left|\overline{\mathcal{M}}(p_1, p_2)\right|^2 \\ \sigma &= \frac{1}{16\pi\left(s - m_{\mathcal{W}}^2\right)^2} \int_{t_{min}}^{t_{max}} \left|\overline{\mathcal{M}}(p_1, p_2)\right|^2 \mathrm{d}t \end{aligned} \tag{2.21}$$

where we emphasize that the matrix element is not constant, but depends on the incoming momenta in a non-trivial way.

We would like to transform these integrals to Monte-Carlo sums. At this stage, with the integration over only one variable, Monte Carlo is inferior to other numerical methods. But as the number of integration variables increases Monte Carlo becomes the superior method. Since we anticipate possible future extensions of this project (e.g. including dark matter emissions), the choice of Monte Carlo is motivated. Following literature ([12], [13], [14], [15], [16]) we see that the Monte Carlo estimate of the eq. (2.20), $\tilde{I}$, is:

$$\tilde{I} = \frac{|t_{max} - t_{min}|}{N} \sum_{i=1}^{N} \left|\overline{\mathcal{M}}(t_i)\right|^2 \tag{2.22}$$

this is readily done by generating t according to a formula of the type: $t_i = r_i(t_{min} - t_{max}) + t_{max}$ where $r_i \in [0, 1)$ is a (pseudo)random number sampled from a flat distribution by a computer. The implementation of this is straightforward, but in general far from optimal. Most importantly, the fact that the numbers t_i are sampled from a flat distribution means that if the integrand ($\left|\overline{\mathcal{M}}(t_i)\right|^2$) is deviating a lot from being flat we get a slow convergence. This can

be seen as follows: assume that the integrand has a peak somewhere in the integration volume and has a much smaller value elsewhere. If it is being sampled at random points then most of those are in the regions where the integrand has a small value. At the same time, it is evident that the largest contribution to the integral is from the peak, while the other regions have a minuscule impact on the total value. The sampling is thus inefficient as it treats all regions equally, not taking into consideration their importance.

A technique that mitigates this inefficiency is called importance sampling. The basic idea is to exploit knowledge about the integrand to sample from a distribution that approximates the integrand. The new integral estimate can have a much better convergence than the plain Monte Carlo (eq. (2.22)), depending on the choice of the new sampling distribution. The basic idea is to perform the following transform ([15]):

$$I = \int f(x)dx = \int \frac{f(x)}{p(x)}p(x)dx = \int \frac{f(x)}{p(x)}dP(x) \tag{2.23}$$

where $f(x)$ is the function we want to integrate and $p(x)$ is the proposal distribution, a probability distribution (pdf)[1] normalized to unity that approximates the behavior of $f(x)$. If we perform the division and the pdf indeed behaves like f, we effectively flatten the integrand thereby reducing the variance. To translate this to MC, we recognize from eq. (2.23) that we need a way of generating samples from the distribution $P(x)$. Then a MC estimate is given by:

$$\tilde{I} = \frac{1}{N}\sum_{i=1}^{N}\frac{f(x_i)}{p(x_i)}|\mathscr{J}(x_i)| \tag{2.24}$$

where the x_i are generated from r_i's, the Jacobian of this transformation is $\mathscr{J}$, and the x_i's are distributed according to $p(x)$.

We want to perform importance sampling on the second integral in eq. (2.21). By examining the formula for the squared matrix element (eq. (2.15)) we see that its dependence on t is t^{-2} from the denominator and there are additional terms with t^1 dependence in the numerator. We try having t^{-1} as the proposal distribution. To this end, we need a way of generating samples distributed accordingly. We shall present later a general algorithm for doing this for any sufficiently well-behaved distribution, but for now we shall derive a analytical way of doing this.

Theorem 1. *For a continuous probability distribution function (pdf) $f(x)$ with the primitive function F, the numbers:*

$$x_i = F^{-1}\left(r_i[F(x_{max}) - F(x_{min})] - F(x_{min})\right) \tag{2.25}$$

are distributed according to f.

The proof is given in appendix B

In the case of interest, we take the pdf to be $f(x) = \frac{C}{x}$, with C being a normalization constant. Then the cdf is $P(x) = C\int_{x_{min}}^{x}\frac{dx'}{x'}$ and $F(x) = \ln(x)$ and we get:

$$\begin{aligned} x_i &= \exp\left(r_i \ln\left(\frac{x_{max}}{x_{min}}\right) + \ln(x_{min})\right) = x_{min}\exp\left(\ln\left(\frac{x_{max}}{x_{min}}\right)^{r_i}\right) = \\ &= x_{min}\left(\frac{x_{max}}{x_{min}}\right)^{r_i} = \frac{x_{max}^{r_i}}{x_{min}^{r_i-1}} \end{aligned} \tag{2.26}$$

[1] We emphasize that the mathematical abbreviation is used where pdf denotes probability distribution function and *not* parton distribution function.

By picking $x_{min} = |t_{max}|$ and $x_{max} = |t_{min}|$ (recall that t is negative so t_{min} is the largest negative value it attains) we can now generate random values of $|t|$ distributed in $[|t_{max}|, |t_{min}|]$ according to $1/|t|$. We get the desired $1/t$ distribution by taking the negative of these values. A MC estimate of the cross-section *eq.* (2.21) with importance sampling of t is thus:

$$\tilde{\sigma} = \frac{\frac{|t_{max}-t_{min}|}{16\pi(s-m_{\mathcal{W}}^2)^2 \cdot N} \sum_{i=1}^{N} \frac{\left|\overline{\mathcal{M}}(t_i)\right|^2}{\frac{1}{t_i}}}{\frac{1}{N}\sum_{i=1}^{N}\left(\frac{1}{t_i}\right)^{-1}} = \frac{|t_{max}-t_{min}|}{16\pi\left(s-m_{\mathcal{W}}^2\right)^2}\sum_{i=1}^{N}\frac{t_i\left|\overline{\mathcal{M}}(t_i)\right|^2}{\mathcal{S}} \tag{2.27}$$

where the lower sum in the first step is the normalization of the proposal distribution (this way we do not need to calculate the normalization constant C, and the t_i's we have for "free" as we generate them anyway). In the second step, the N's cancel and we denote the normalization sum by $\mathcal{S}$.

3 Event Generator Implementation

We now move on to describing how the event generator is realized in the code. The event generator was programmed entirely by the author and can be found at [2]. Since the final version of the event generator actually has more features than those described above, we first outline how the hitherto presented theory was implemented in the first versions. We then expand upon the theory.

The event generator is initialized with the angle cut, the number of events to be created, the mass and charge of the metal nucleus, the electron beam energy and metal thermal momentum:

```
#initiate: tungsten mass (in GeV), tungsten charge, number of events to be
#created, and lists [electronArgs], [metalArgs] and the cut on the angle
events=eventGenerator(180, 74, 100000, electronArgs, metalArgs,
electronDistribution, metalDistribution, angleCut)
```

The program goes on to create and boost the four-momenta of the electrons and metals to the CM frame. Using them, the Lorentz factor γ and the centre of momentum velocity v_{CM} can be calculated according to eq. (2.3). As stated earlier, in the code the quantity $|t|$ is used in favor of t (this amounts to changing a couple of signs in the formulas presented in the earlier sections). The max and min value of $|t|$ is determined using $|t|_{max} = 4E_1^2$ and eq. (A.33), respectively. The $|t|$ is generated randomly but according to the $1/|t|$ distribution. The matrix element squared is calculated according to eq. (2.15), it is multiplied with all the relevant factors according to eq. (2.27) and it is saved for later cross-section calculation:

```
self.matrixEs.append(tAbs[j]*jacobian*self.matrixElement(s,tAbs[j],u)/(16*
math.pi*self.kinematicFcn(s, 0, self.mSq)))
```

The $|t|$ is used to obtain the angle θ and the trivial azimuthal angle ϕ is generated randomly (c.f. Figure 3). With these parameters, the outgoing momenta can be calculated according to eq. (2.5) and boosted back to LAB frame using eq. (2.7):

```
self.generate34(j, p1[0], p2[0], theta, phi) #calculates p3,p4 in CM frame
self.boostBack(j, gamma, vCM, p1[0], p2[0], theta)
```

This is done for as many electron - metal pairs as specified by the number of events parameter. Desired plots can now be plotted using saved quantities, and the cross-section $\tilde{\sigma}$ is now calculated

using eq. (2.27). Finally, a plain MC estimate is calculated using eq. (2.22) and presented alongside $\tilde{\sigma}$.

With this, the event generator is functioning and can be used for simulations. But we would like to expand this to allow for more precise and realistic modelling. For example, the massive tungsten nucleus does not behave like a point charge for a $\mathcal{O}(10)$ GeV electron and thus we would like to include a form factor in the matrix element. Furthermore, the electrons in the incident beam are not all going to have the same energy, but rather their energy is going to be distributed around the target value. A similar argument applies to the metal thermal momenta. We thus want to begin the program with distributing the electron and tungsten momenta (or equivalently-energies) according to some user specified distribution function.

We can not expect that this distribution will be easily integrable and invertible so that Theorem 1 can be easily applied. Therefore we need a new way of generating samples according to a specified distribution. We present it as "Algorithm 1, Sampling algorithm" below. The algorithm is implemented in the code and was provided by J. Bellm [17]. Its objective is to distribute variables x_i according to $f(x)$ in the interval $[x_{min}, x_{max}]$. The sampling algorithm

Algorithm 1 Sampling Algorithm

Divide the interval between x_{max} and x_{min} into N equal bins.
Create a list, "probs", which stores the relative probabilities of each bin. Initially the same for all bins.
Create a list, "H", which will contain the samples.
The function $f(x)$ is the pdf of the desired distribution.
while len(H)< (number of events) **do**
  choose a bin randomly but taking into account their relative probability, call it i
  choose x flat in bin i
  if $f(x)$ >probs[i] **then**
    increase the probability of bin i
    reset H
  end if
  if random()< $f(x)$/probs[i] **then**
    H.append(x)
  end if
end while

was implemented in the code, and was used to distribute the incoming electron and tungsten momenta according to a Gaussian distribution:

$$f(E_j) = \frac{1}{\sigma_j\sqrt{2\pi}} \exp\left(-\frac{(E_j - \overline{E}_j)^2}{2\sigma_j^2}\right) \tag{3.28}$$

where the index j is either e for the electrons or $\mathcal{W}$ for tungsten, σ_j is the standard deviation and $\overline{E}_j$ is the mean. The mean is taken to be the target beam energy for the electrons and 0 for tungsten as in the Lab frame the tungsten is equally likely to move in the positive and negative z-direction due to thermal motion. The result of having the incoming momenta distributed is that s is no longer a constant. Therefore, the flux factor in eq. (2.27) has now to be taken inside the sum as it is in general different for each term.

What values of $\sigma_{\mathcal{W}}$ should we use? We need to translate temperatures of the metal target into momenta of individual nuclei. In practice this is a very complicated problem, but we want just

an order-of-magnitude estimate to determine the effects of this on the observable quantities. Guided by [18] we use the harmonic oscillator approximation to estimate the tungsten momenta. As a harmonic oscillator, the nucleus will have at most $E = \frac{3}{2} m_{\mathcal{W}} v^2$ kinetic energy and from the equipartition theorem we know this equals to $\frac{3}{2} k_B T$ (the three in both expression comes from the three spatial dimensions it can oscillate in). Here, k_B is the Boltzmann's constant and T is the temperature of the target. We get:

$$\frac{3}{2} k_B T = \frac{3}{2} m_{\mathcal{W}} v^2 = \frac{3p^2}{2m_{\mathcal{W}}} \Rightarrow p = \sqrt{k_B m_{\mathcal{W}} T} \tag{3.29}$$

for $T = 300, 800, 3500$ K ($\approx$ room temperature, 500°C and close to the melting point of tungsten) this gives $p \approx 70, 100, 200$ keV/c.

Meaningful values of σ_e can be obtained by consulting literature. The LEP experiment reported values of 2 MeV [19]. In contrast, the LDMX experiment is considering far greater smearings. From [3] (figure 37) we read off a smearing of $\approx$0.05 GeV. Hence, the value used throughout the plots, 0.01 GeV is certainly reasonable. The three values considered when comparing the effects of the smearings, 0.01, 0.03 and 0.1 GeV, are also well motivated as they cover the region interesting for LDMX.

We are using the approximation that the tungsten only has thermal momentum in the z-direction. For real thermal momenta there would of course on average be equal motion in the x and y directions. However, we just saw that the thermal momenta are at least four orders of magnitude lower than the beam momenta. Hence, we expect the effects of the thermal motion to be very small. Furthermore, the kinematics would become more cumbersome, therefore we confine ourselves to this approximation.

4 Validation and Testing

We want to validate that the different modifications we added to the plain Monte Carlo (eq. (2.22)), i.e. the importance sampling and the distribution of the initial momenta yield meaningful results. Firstly, we need to verify that the importance sampling gives the same answer as the plain Monte Carlo (within the statistical variance) when the initial momenta are static. Secondly, we want to observe that in the limit when the standard deviation of the electron and tungsten distributions goes to zero, we get the same result as in the plain Monte Carlo.

We perform the following procedure: at a given beam energy, we make ten runs of the program with 10^5 events each. Every time we record the cross-section of both the plain MC and MC with importance sampling. We present this as an average of the 10 values ($\overline{\sigma}$) with the error given by the difference between those values of cross-section that deviate the most from $\overline{\sigma}$. We then enable the distribution of initial momenta and repeat the procedure. We do this with a very small standard deviation ($\sigma_e, \sigma_{\mathcal{W}} = 0.001$ GeV) to test the limit when the Gaussian approaches a delta distribution. The effects of more realistic values of the standard deviation are examined in the Results section.

Table 1: *Comparison of plain MC, MC enhanced with importance sampling with fixed initial momenta and with initial momenta distributed according to a Gaussian. Cut on angle: 20°.*

Energy $\overline{E}_e$ [GeV]	Plain MC $\overline{\sigma}$ [μb]	Importance S. $\overline{\sigma}$ [μb]	Distributed M. $\overline{\sigma}$ [μb]
30	$11.1^{+0.2}_{-0.1}$	$11.1^{+0.1}_{-0.1}$	$11.1^{+0.1}_{-0.1}$
8	160^{+2}_{-2}	159^{+1}_{-1}	159^{+1}_{-1}
4	638^{+5}_{-8}	640^{+5}_{-5}	641^{+4}_{-4}

From table 1 we see that all methods agree within statistical error. In particular, notice the lower error on the importance sampling results. This is exactly the variance reduction we discussed in section 2.4. We now go on to perform a second test. We make 100 runs of the code (each producing 10^5 events) and histogram the cross-sections. Since we are using MC, we expect a Gaussian distribution where the plain MC has a larger variance than importance sampling. We then repeat the process but now with incoming momenta distributed according to a Gaussian (with $\sigma = 0.001$ GeV) in addition to the importance sampling (just as for the previous test). We calculate the corresponding average and standard deviation of the histograms, see table 2.

Table 2: *Comparison of plain MC, MC enhanced with importance sampling with fixed initial momenta and with initial momenta distributed according to a Gaussian. Values obtained by making 100 runs of the code and histogramming the resulting cross-sections.* $\overline{E}_e = 4$ *GeV, cut on angle 20°. Standard D. denotes standard deviation i.e. square root of the variance.*

Quantity	Plain MC	Importance S.	Distributed M.
$\overline{\sigma}$ [μb]	639	640	639
Standard D. [μb]	7	4	4

The results in table 2 confirm our findings from table 1. In addition, the data is presented in fig. 6 and fig. 7. There we can clearly see the expected Gaussian shape of the histograms. In particular, the variance reduction between plain MC and importance sampling is striking.

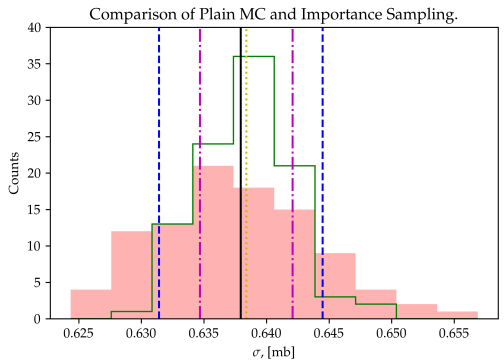

Figure 6: Histogram of 100 values of σ obtained using plain MC (filled red, standard deviation: dashed blue line, average: solid black) and with importance sampling (green steps, standard deviation: dot-dashed magenta, average: yellow dotted line).

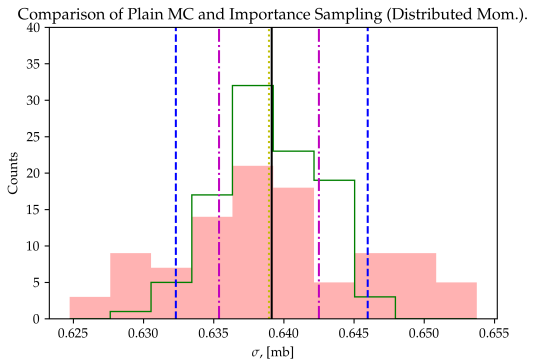

Figure 7: Histogram of 100 values of σ obtained using plain MC (filled red, standard deviation: dashed blue line, average: solid black) and with importance sampling with distributed incoming momenta (green steps, standard deviation: dot-dashed magenta, average: yellow dotted line).

5 Results

We now present the final results of the project. All plots that follow were created with 10^5 events. The smearing used is 70 keV for tungsten (as discussed earlier, this corresponds to room temperature) and 0.01 GeV for electrons unless stated otherwise. Figures 8 through 11 show the differential cross section $\frac{d\sigma}{d|t|}$, i.e. the histogram of the terms in the Monte Carlo sum that computes the estimate of the cross-section. Note that despite looking similar, the scales ($|t|$-axis) are very different. The Figures 12 to 15 show the outgoing electron energy distribution in the Lab frame. The effects of the Gaussian distribution of the initial momenta can be clearly seen as deformations of the $1/|t|$ shape that would be expected, had the initial momenta had a fixed value. It is evident that the effect is largest for small electron beam energies, and barely visible in the highest energy plot (Figure 15). This is expected since the relative variation brought about by the Gaussian distribution is greater the lower the beam energy is.

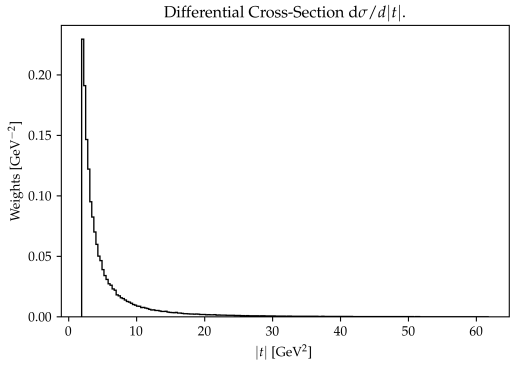

Figure 8: Differential cross-section $\frac{d\sigma}{d|t|}$, the cut on the angle is 20°, $\sigma_e = 0.01$ GeV, $\sigma_{\mathcal{W}} = 70$ keV and $\overline{E}_e = 4$ GeV.

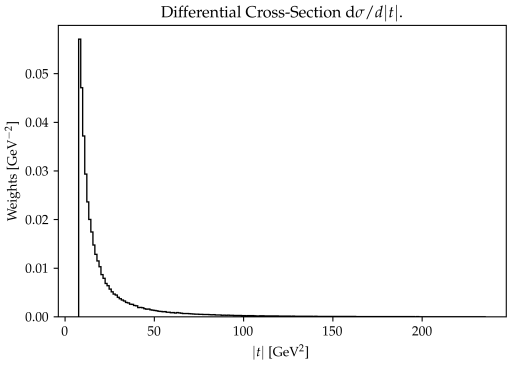

Figure 9: Differential cross-section $\frac{d\sigma}{d|t|}$, the cut on the angle is 20°, $\sigma_e = 0.01$ GeV, $\sigma_{\mathcal{W}} = 70$ keV and $\overline{E}_e = 8$ GeV.

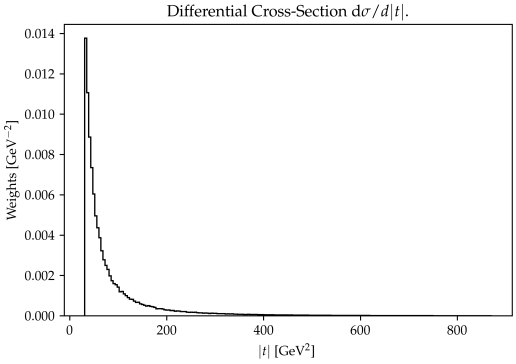

Figure 10: Differential cross-section $\frac{d\sigma}{d|t|}$, the cut on the angle is 20°, $\sigma_e = 0.01$ GeV, $\sigma_{\mathcal{W}} = 70$ keV and $\overline{E}_e = 16$ GeV.

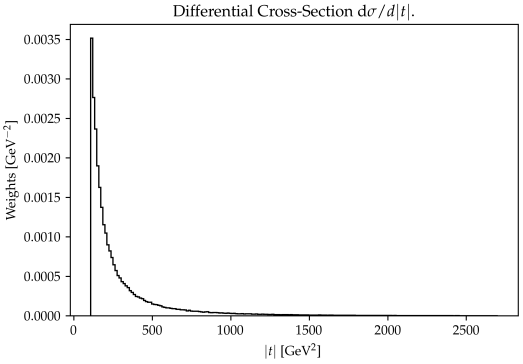

Figure 11: Differential cross-section $\frac{d\sigma}{d|t|}$, the cut on the angle is 20°, $\sigma_e = 0.01$ GeV, $\sigma_{\mathcal{W}} = 70$ keV and $\overline{E}_e = 30$ GeV.

In Figure 16 we see how the cuts on allowed angles affect their overall distribution. The fact that the histograms do not overlap is expected, as all plots were made with equal number of events but the max angle (back-scattering) is the same. Figure 17 how $\frac{d\sigma}{d\theta_L}$ is affected by the beam

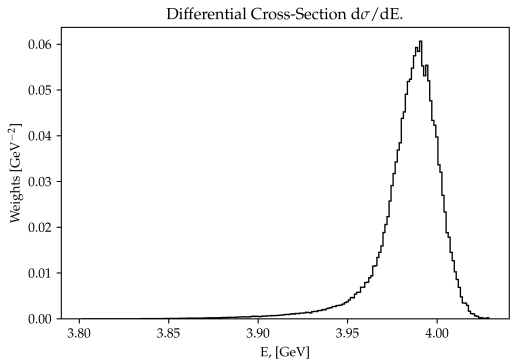

Figure 12: Differential cross-section $\frac{d\sigma}{dE}$ where E is the energy of the outgoing electron. The cut on the angle is 20°, $\sigma_e = 0.01$ GeV, $\sigma_{\mathcal{W}} = 70$ keV and $\overline{E}_e = 4$ GeV.

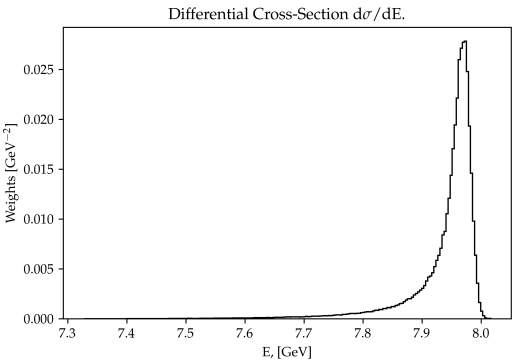

Figure 13: Differential cross-section $\frac{d\sigma}{dE}$ where E is the energy of the outgoing electron. The cut on the angle is 20°, $\sigma_e = 0.01$ GeV, $\sigma_{\mathcal{W}} = 70$ keV and $\overline{E}_e = 8$ GeV.

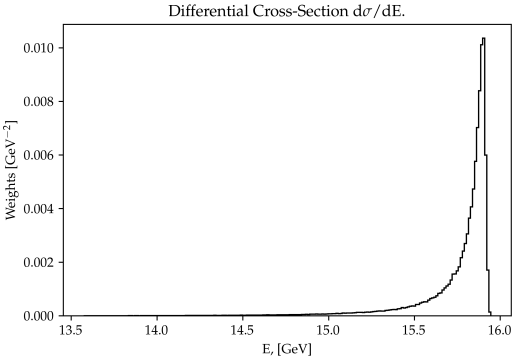

Figure 14: Differential cross-section $\frac{d\sigma}{dE}$ where E is the energy of the outgoing electron. The cut on the angle is 20°, $\sigma_e = 0.01$ GeV, $\sigma_{\mathcal{W}} = 70$ keV and $\overline{E}_e = 16$ GeV.

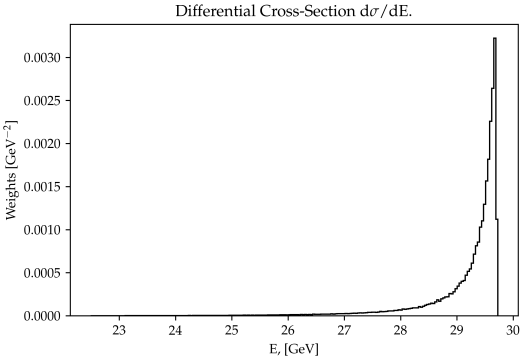

Figure 15: Differential cross-section $\frac{d\sigma}{dE}$ where E is the energy of the outgoing electron. The cut on the angle is 20°, $\sigma_e = 0.01$ GeV, $\sigma_{\mathcal{W}} = 70$ keV and $\overline{E}_e = 30$ GeV.

energy. The last figures (18-23) show how different values of σ affect measurable quantities. In order to test the effects of the smearing of the initial tungsten and electron momenta, the following test was performed: the tungsten energy was fixed (no distribution) while the electron beam was distributed with σ_e =0.01, 0.03, 0.1 GeV each time producing 10^5 events. This was then repeated for the tungsten with $\sigma_{\mathcal{W}} = 70, 100, 200$ keV. These values where obtained and explained in section 3. From Figures 18 and 22 we see that the differential cross sections $d\sigma/d\theta_L$ show no visible changes. Also figure 23 shows no noticeable changes, the conclusion is that changes due to the temperature of the tungsten are very small. In Figures 19 however, we can see alterations that are due to the smearing of the electron momentum. We see how even small values of σ_e drastically change the distribution of the outgoing momenta. At $\sigma_e = 0.1$ GeV the histogram basically looks like a Gaussian, making any search for e.g. dark matter very difficult. Even the smaller values of σ_e cause significant changes to the distribution. Depending on the momentum spread, the distribution gets extra counts and bins on the edges. This could interfere with searches for rare events. One of the proposed experiments for LDM search, LDMX, is supposed to utilize the same electron-nucleus scatterings to search for dark matter that we have been describing [3]. We borrow one of the figures from [3] and present in fig. 20 together

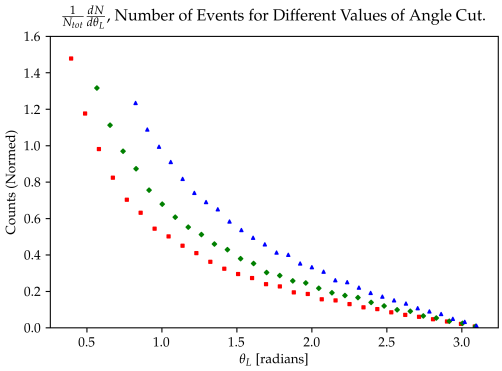

Figure 16: The scattering angle θ in Lab frame, for three different runs with angle cuts 20°(red squares), 30°(green diamonds) and 45°(blue triangles). $\overline{E}_e$= 8 GeV.

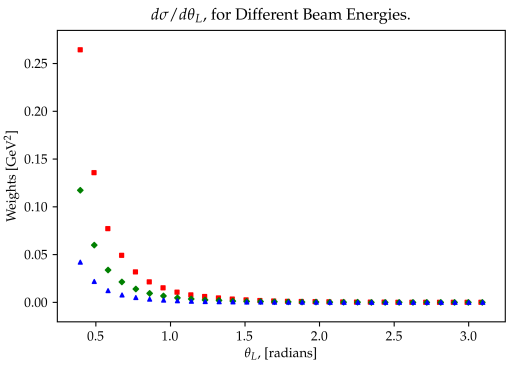

Figure 17: The differential cross-section $d\sigma/d\theta_L$, for different beam energies $\overline{E}_e$=4 (red squares), 6 (green diamonds) and 10 (blue triangles) GeV. The angle cut is 20°.

with an zoomed-in version of fig. 19: fig. 21. Note how as we move leftwards in fig. 20, the hypothetical dark matter signal is initially only sightly divergent from the electron background (the vertical scale is logarithmic). This means that even a small excess of events such as the one brought about by the electron smearing could easily drown out such a signal.

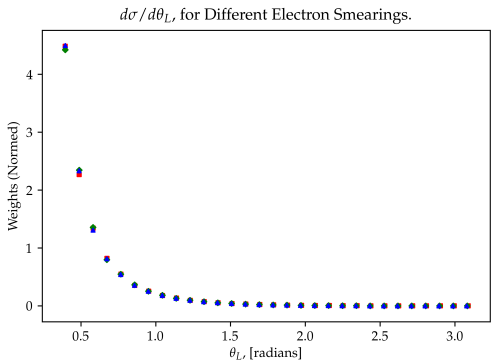

Figure 18: Differential cross-section $\frac{d\sigma}{d\theta_L}$ for different electron smearings. $\overline{E}$ = 4 GeV, σ_e =0.01 (red squares), 0.03 (green diamonds), 0.1 (blue triangles) GeV. $\sigma_{\mathcal{W}} = 0$.

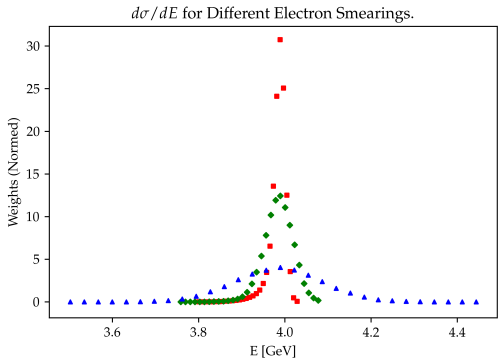

Figure 19: Differential cross-section $\frac{d\sigma}{dE}$ where E is the energy of the outgoing electron, for different electron smearings. $\overline{E}$ = 4 GeV, σ_e =0.01 (red squares), 0.03 (green diamonds), 0.1 (blue triangles) GeV. $\sigma_{\mathcal{W}} = 0$.

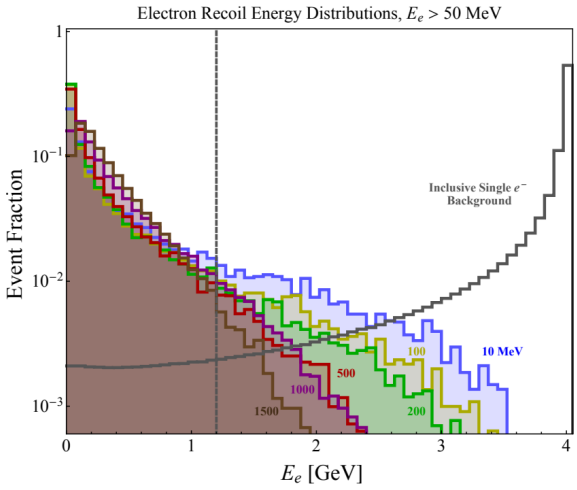

Figure 20: Expected dark matter signals at LDMX [3]. Colored (filled) histograms depict LDM signals, the numbers denote the corresponding LDM particle mass. The transparent histogram depicts the expected electron background.

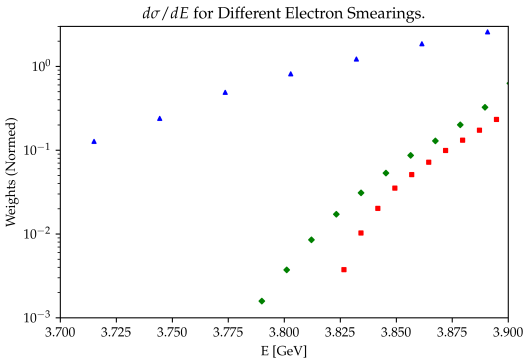

Figure 21: Zoomed-in version of fig. 19, provided for comparison with the LDMX figure. Notice the logarithmic vertical scale.

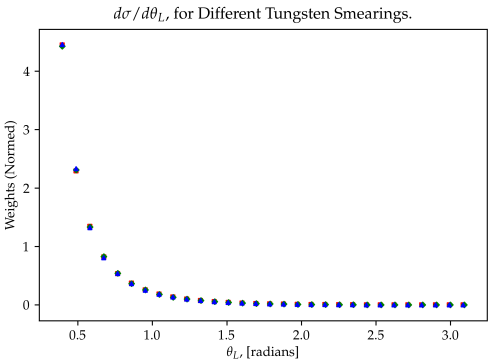

Figure 22: Differential cross-section $\frac{d\sigma}{d\theta_L}$ for different tungsten smearings. $\overline{E} = 4$ GeV, $\sigma_{\mathcal{W}}$ =70 (red squares), 100 (green diamonds), 200 (blue triangles) keV. $\sigma_e = 0$.

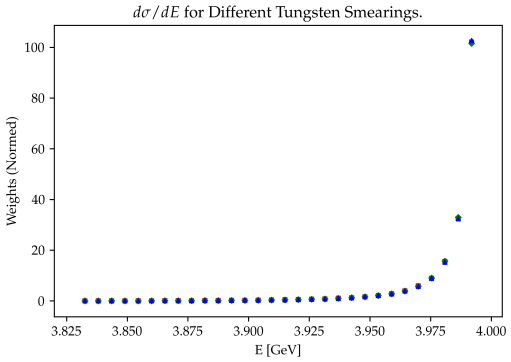

Figure 23: Differential cross-section $\frac{d\sigma}{dE}$ where E is the energy of the outgoing electron, for different tungsten smearings. $\overline{E} = 4$ GeV, $\sigma_{\mathcal{W}}$ =70 (red squares), 100 (green diamonds), 200 (blue triangles) keV. $\sigma_e = 0$.

6 Conclusion

We have demonstrated how an event generator can be constructed for the relevant t-channel scattering. The relevant kinematics was developed, Feynman rules were used to obtain the matrix element and Monte Carlo techniques provided the means to calculate the cross-sections.

In order to reduce variance and hence improve convergence, the technique of importance sampling was included. By taking advantage of the known form of the matrix element, we were able to find a function that indeed reduced the statistical fluctuations.

The event generator was furthermore equipped with the ability to distribute the initial momenta

according to a Gaussian. This allows for simulation of thermal motions of the metal target and the fact that electrons in a beam do not have uniform energy. The code (that can be found at [2]) can simulate any sufficiently well-behaved distribution, and thus a simple modification to the code allows the user to model the distribution of their choosing. In addition, a form factor could also be included with minimal modifications. Apart from these modifications, the next step in developing the generator would be to include the emission of dark matter (emission of A' from the scattered electron).

A number of tests were performed in order to validate the aforementioned modifications against the simplest version of the generator. The tests showed that both importance sampling and distribution of initial momenta agree with plain Monte Carlo in the relevant limits.

We examined the effects of the initial distribution of momenta and comparing them to the proposed LDMX experiment. We concluded that the thermal motions of tungsten have little impact on the observables. The spread of the beam energies could however have a significant impact on the sensitivity to potential dark matter signals. However, given the crude scattering model used and the lack of a form factor additional improvements are necessary before any definitive conclusions can be made.

A Relationship between the scattering angle and t_{max}

As discussed previously, we want an expression of t_{max} in terms of the electron scattering angle in the Lab frame. First, we note that the outgoing electron momentum is in the Lab frame:

$$\mathbf{p}_{L,e} = (P^* \sin(\theta)\cos(\phi), P^* \sin(\theta)\sin(\phi), \gamma P^*(\cos(\theta) + v_{CM})) \tag{A.30}$$

where the x, y components are the same as in the CM frame as they are orthogonal to the Lorentz boosts. The z component is given by eq. (2.7). From the spherical coordinate geometry (Figure 3) we see that the scattering angle in the Lab frame is $\theta_L = \arctan\left(\frac{\sqrt{\mathrm{p_x}^2+\mathrm{p_y}^2}}{\mathrm{p_z}}\right)$. The scattering angle in the CM frame depends on t, hence we want to solve for t as a function of θ_L. We have that:

$$\begin{aligned}
\tan(\theta_L) &= \frac{\sqrt{((P^*)^2 \sin^2\theta(\cos^2\phi + \sin^2\phi))}}{\gamma P^*(\cos\theta + v_{CM})} = \frac{\sin\theta}{\gamma(\cos\theta + v_{CM})} \Leftrightarrow \\
\frac{1}{\tan\theta_L} &= \gamma\left(\frac{\cos\theta + v_{CM}}{\sin\theta}\right) = \left(\frac{\frac{2st}{(s-m_{\mathcal{W}}^2)^2} + 1 + v_{CM}}{\sqrt{1 - \left(\frac{2st}{(s-m_{\mathcal{W}}^2)^2} + 1\right)^2}}\right)
\end{aligned} \tag{A.31}$$

where we used the expression for θ (CM scattering angle) in terms of invariant quantities (eq. (2.6)) and in the last line that $\sin\theta = \sqrt{1-\cos^2\theta}$. Denoting $\left(s - m_{\mathcal{W}}^2\right)^2$ by λ, rearranging and simplifying gives:

$$\begin{aligned}
0 &= \gamma^2 \tan^2\theta_L \left(1 + v_{CM}^2 + 2v_{CM} + \frac{4s}{\lambda}\left(t^2\left(\frac{s}{\lambda} + \frac{s}{\lambda\gamma^2\tan^2\theta_L}\right) + t\left(1 + v_{CM} + \frac{1}{\gamma^2\tan^2\theta_L}\right)\right)\right) = \\
&= \gamma^2\tan^2\theta_L\left(1 + v_{CM}^2 + 2v_{CM} + \frac{4s}{\lambda}\left(t^2\zeta + 1\xi\right)\right)
\end{aligned} \tag{A.32}$$

we recognize this as a second degree equation in t, which can immediately be solved:

$$t = -\frac{\xi}{2\zeta} \pm \sqrt{\frac{1}{4}\left(\frac{\xi}{\zeta}\right)^2 - \frac{\lambda}{4s\zeta}\left(1 + v_{CM}^2 + 2v_{CM}\right)} \tag{A.33}$$

B Proof of Theorem 1

Here we set out to prove Theorem 1. First, recall the theorem:

Theorem 1. *For a continuous probability distribution function (pdf) $f(x)$ with the primitive function F, the numbers:*

$$x_i = F^{-1}\left(r_i[F(x_{max}) - F(x_{min})] - F(x_{min})\right) \tag{B.1}$$

are distributed according to f.

Proof. Suppose that the pdf is normalized on the interval $[x_{min}, x_{max}]$ and has the primitive function $F(x)$. Then its cumulative distribution function (cdf) is given by $P : [x_{min}, x_{max}] \to [0,1]$, $P : x \mapsto \int_{x_{min}}^{x} f(x')dx'$ and it takes values between 0 and 1. It is also injective by definition. Hence, there exists a number $r \in [0,1]$ s.t.:

$$P(x) = \int_{x_{min}}^{x} f(x')dx' = r\int_{x_{min}}^{x_{max}} f(x')dx' \tag{B.2}$$

utilizing the existence of the inverse and primitive function we get:

$$\begin{aligned} &F(x) - F(x_{min}) = r\left(F(x_{max}) - F(x_{min})\right) \Leftrightarrow F(x) = r\left(F(x_{max}) - F(x_{min})\right) + F(x_{min}) \\ &\Leftrightarrow x = F^{-1}\left(r(F(x_{max}) - F(x_{min})) + F(x_{min})\right) \end{aligned} \tag{B.3}$$

which is just eq. (B.1). We also need to show that the numbers x are indeed distributed according to f. Hence, we want to show that $\frac{\mathrm{d}P}{\mathrm{d}x} = f$. This follows from the definition for the LHS of eq. (B.2), while for the RHS:

$$\frac{\mathrm{d}P}{\mathrm{d}x} = \frac{\mathrm{d}P}{\mathrm{d}r}\frac{\mathrm{d}r}{\mathrm{d}x} = \frac{\mathrm{d}\left[r\left(F(x_{max}) - F(x_{min})\right)\right]}{\mathrm{d}r}\frac{\mathrm{d}r}{\mathrm{d}x} = \left(F(x_{max}) - F(x_{min})\right)\frac{1}{\frac{\mathrm{d}x}{\mathrm{d}r}} \tag{B.4}$$

From the last line of eq. (B.3) we get that (denoting the argument of F^{-1} by ϑ):

$$\frac{\mathrm{d}x}{\mathrm{d}r} = \frac{\mathrm{d}F^{-1}(\vartheta)}{\mathrm{d}\vartheta}\frac{\mathrm{d}\vartheta}{\mathrm{d}r} = \left[F(x_{max}) - F(x_{min})\right]\left(\frac{\mathrm{d}F(x)}{\mathrm{d}x}\right)^{-1} \tag{B.5}$$

where we used the result from elementary analysis that:

$$\frac{\mathrm{d}F^{-1}(\vartheta)}{\mathrm{d}\vartheta} = \left(\frac{\mathrm{d}F(F^{-1}(\vartheta))}{\mathrm{d}x}\right)^{-1} = \left(\frac{\mathrm{d}F(x)}{\mathrm{d}x}\right)^{-1} \quad \text{If} \quad F^{-1}(\vartheta) = x \tag{B.6}$$

but this is just $(f)^{-1}$, so inserting eq. (B.5) into eq. (B.4) gives us that also the RHS of eq. (B.3) is equal to f. This concludes the proof. ■

References

[1] E. Izaguirre, G. Krnjaic, P. Schuster and N. Toro, Phys. Rev. D **90** (2014) no.1, 014052 doi:10.1103/PhysRevD.90.014052 [arXiv:1403.6826 [hep-ph]].

[2] M. Nowak. A Simple Event Generator [Online]. 2019. https://gitlab.com/MichalNowak0/a-simple-event-generator

[3] T. Åkesson *et al.* [LDMX Collaboration], arXiv:1808.05219 [hep-ex].

[4] B. Holdom, Phys. Lett. **166B** (1986) 196. doi:10.1016/0370-2693(86)91377-8

[5] Ellis, Joshua P. "TikZ-Feynman: Feynman diagrams with TikZ." Computer Physics Communications 210 (2017): 103-123. doi:10.1016/j.cpc.2016.08.019 arXiv:1601.05437

[6] M. E. Peskin, D. V. Schroeder, An Introduction to Quantum Field Theory (Westview Press, 2016)

[7] V. Shtabovenko, R. Mertig and F. Orellana, "New Developments in FeynCalc 9.0", Comput. Phys. Commun., 207, 432-444, 2016, arXiv:1601.01167.

[8] R. Mertig, M. Böhm, and A. Denner, "Feyn Calc - Computer-algebraic calculation of Feynman amplitudes", Comput. Phys. Commun., 64, 345-359, 1991.

[9] R. H. Helm, Phys. Rev. **104** (1956) 1466. doi:10.1103/PhysRev.104.1466

[10] J. Engel, Phys. Lett. B **264** (1991) 114. doi:10.1016/0370-2693(91)90712-Y

[11] J. Bramante, P. J. Fox, G. D. Kribs and A. Martin, Phys. Rev. D **94** (2016) no.11, 115026 doi:10.1103/PhysRevD.94.115026 [arXiv:1608.02662 [hep-ph]].

[12] E. Byckling, K. Kajantie, Particle Kinematics (John Wiley & Sons, 1973)

[13] A. Doucet, N. de Freitas, N. Gordon *et al.*, Sequential Monte Carlo Methods in Practice (Springer 2001)

[14] C. P. Robert and G. Casella, Monte Carlo Statistical Methods (Springer 1999)

[15] S. Weinzierl, Introduction to Monte Carlo methods, arXiv:0006269v1 [hep-ph] (2000)

[16] F, James. Monte Carlo Phase Space [Online]. 1968. https://cds.cern.ch/record/275743/files/CERN-68-15.pdf

[17] J. Bellm. Introduction to Monte-Carlo Event Generators (MC) [Online]. 2018. http://home.thep.lu.se/ jbellm/VSOP/

[18] P. Hofmann, Solid State Physics-An Introduction (Wiley-VCH Verlag, 2015)

[19] R. Assmann *et al.* [Working Group on LEP Energy], Z. Phys. C **66** (1995) 567. doi:10.1007/BF01579631